Preprints.org

Article

Not peer-reviewed version

Solution Induced Degradation of the Silicon Nanobelt Field Effect Transistor Biosensors

Jung-Chih Lin , Zhao-Yu Zhou , Yi-Ching Cheng , I-Nan Chang , Chu-En Lin * , Chi-Chang Wu *

Posted Date: 7 December 2023

doi: 10.20944/preprints202312.0419.v1

Keywords: silicon nanobelt; NBFET; nanobelt biosensor; degradation; ions penetration; surface functionalization

Preprints.org is a free multidiscipline platform providing preprint service that is dedicated to making early versions of research outputs permanently available and citable. Preprints posted at Preprints.org appear in Web of Science, Crossref, Google Scholar, Scilit, Europe PMC.

Copyright: This is an open access article distributed under the Creative Commons Attribution License which permits unrestricted use, distribution, and reproduction in any medium, provided the original work is properly cited.

Preprints (www.preprints.org) | NOT PEER-REVIEWED | Posted: 7 December 2023 doi:10.20944/preprints202312.0419.v1

Disclaimer/Publisher's Note: The statements, opinions, and data contained in all publications are solely those of the individual author(s) and contributor(s) and not of MDPI and/or the editor(s). MDPI and/or the editor(s) disclaim responsibility for any injury to people or property resulting from any ideas, methods, instructions, or products referred to in the content.

Article

Solution Induced Degradation of the Silicon Nanobelt Field Effect Transistor Biosensors

Jung-Chih Lin [1], Zhao-Yu Zhou [2], Yi-Ching Cheng [2], I-Nan Chang [3], Chu-En Lin [2,*] and Chi-Chang Wu [2,*]

[1] Department of Integrated Chinese and Western Medicine, Chung Shan Medical University Hospital, and School of Medicine, Chung Shan Medical University, Taichung 40201, Taiwan; cshy1027@csh.org.tw

[2] Department of Electronic Engineering, National Chin-Yi University of Technology, Taichung 411030, Taiwan; coco1113411012@gmail.com (ZY Zhou), arthur@link-win.com (YC Cheng), celin@ncut.edu.tw (CE Lin), ccwu@ncut.edu.tw (CC Wu)

[3] Department of Electronic Engineering, Feng Chia University, Taichung 40724, Taiwan; enchung@fcu.edu.tw

* Correspondence: celin@ncut.edu.tw, ccwu@ncut.edu.tw

Abstract: Field-effect transistor (FET)-based biosensors stand as powerful analytical tools for detecting trace-specific biomolecules in diverse sample matrices, especially in the realms of pandemics and infectious diseases. The primary concern in applying these biosensors is their stability, a factor directly impacting the accuracy and reliability of sensing over extended durations. The risk of biosensor degradation is substantial, potentially jeopardizing sensitivity and selectivity and leading to inaccurate readings, including the possibility of false positives or negatives. This paper delves into the documented degradation of silicon nanobelt FET (NBFET) biosensors induced by buffer solutions. The results highlight a positive correlation between immersion time and the threshold voltage of NBFET devices. Secondary ion mass spectrometry analysis demonstrates a gradual increase in sodium and potassium ion concentrations within the silicon as immersion days progress. This outcome is ascribed to the nanobelt's exposure to the buffer solution during the biosensing period, enabling ion penetration from the buffer into the silicon. The study emphasizes the critical need to address buffer solution-induced degradation to ensure the long-term stability and performance of FET-based biosensors in practical applications.

Keywords: silicon nanobelt; NBFET; nanobelt biosensor; degradation; ions penetration; surface functionalization

1. Introduction

Biosensors are analytical devices that integrate biological recognition elements with transducers to detect and quantify specific analytes in various sample matrices [1–3]. These devices are widely used in a range of applications, including disease detection, medical diagnostics, drug selection, and environmental monitoring [4–7]. Recently, biosensors based on semiconductor materials is attracting more and more attention. This kind of biosensors offer numerous advantages over traditional analytical techniques, including high sensitivity, high specificity, and miniaturing capability [8,9].

Numerous two-dimensional (2D) semiconductor materials, such as nanowires, nanobelts, and nanotubes, find application in biosensing [10–14]. The 2D materials are used in the devices serving as the transmission channel of carriers, and transducer devices employing these materials have demonstrated exceptional properties for detecting trace biomolecules, showcasing ultrahigh sensitivity. However, the critical challenge lies in addressing the stability and potential degradation induced by the solution when operating, given that these materials are exposed to ionic solutions [15,16]. Ensuring the accurate and reliable performance of biosensors over extended periods becomes imperative, despite their ultrahigh sensitivity. Solution-induced stability and degradation of biosensors made from 2D materials necessitate careful consideration, emphasizing the need to develop strategies that safeguard their performance in the presence of ionic solutions.

© 2023 by the author(s). Distributed under a Creative Commons CC BY license.

Preprints (www.preprints.org) | NOT PEER-REVIEWED | Posted: 7 December 2023 doi:10.20944/preprints202312.0419.v1

Biomedical sensors are designed to detect trace biomolecules within solutions, which can comprise various body fluids like blood, serum, urine, or buffered solutions [17,18]. These biosensors are subject to degradation over time due to various factors, including environmental conditions, surface chemistry, and biological interactions. Surface chemistry is one of the critical factors that can affect the stability of biosensors. The surface chemistry of the transducer material can significantly influence the interaction between the biological recognition element and the analyte [19]. The adsorption of proteins, nucleic acids, and other biomolecules onto the transducer surface can interfere with the sensing mechanism and cause false reading results.

Stability issue stands as a pivotal concern when considering the performance of a transistor device. This concern becomes particularly pronounced when dealing with biosensor devices, as they are frequently employed in liquid environments. Unlike conventional transistor devices that typically operate in controlled environments safeguarded against moisture, light, and magnetic interference, biosensors must function within the context of trace biomolecule detection in solutions. These solutions often comprise various body fluids, such as blood, serum, urine, or buffer solutions. The extended immersion of biosensors in such solutions can accelerate the degradation of the transistor device itself, or even lead to the deterioration of its surface functionalization [20,21]. What further compounds the challenge is the high ion concentration present in these body fluids or buffer solutions. When a semiconductor biosensor device is immersed in such solutions, these ions can permeate the device, raising concerns related to the device's reliability [22,23].

In light of these considerations, it becomes imperative to conduct a time-dependent stability assessment of the 2D materials based biosensors when immersed in a buffer solution. Such an evaluation is vital to ascertain the device's ability to maintain consistent and reliable performance over time. Literature concerning about the solution induced stability is, however, little reported. Therefore, this study aims to uncover the longevity and resilience of the biosensor device when subjected to the complex and dynamic conditions of a liquid environment.

This paper details the fabrication of a silicon nanobelt field effect transistor (NBFET) device using a commercially available CMOS-compatible manufacturing technique. Diverging from traditional Planar FET devices, the NBFET employs a narrow and thin nanobelt as a channel to establish the connection between the source and drain. This unique design imparts ultrahigh sensitivity to the NBFET biosensor, particularly in the detection of biomolecules. The fabricated NBFET device was specifically employed for the detection of DNA strands. Subsequently, this NBFET biosensor underwent immersion in a buffer solution, and its electrical properties were systematically monitored to assess the solution-induced stability of the device. The investigation into the device's performance over prolonged periods in challenging environments provides valuable insights into its durability and efficacy as a stable and robust sensing tool. The outcomes of this study not only contribute to the broader field of biosensors but also establish a foundational reference for future advancements in biomedical devices. By elucidating the solution-induced stability of the NBFET biosensor, this research paves the way for improved understanding and innovation in the development of reliable and enduring sensing technologies for various biomedical applications.

2. Materials and Methods

A side-gated NBFET was fabricated and applied as the biosensor device. The sensor was completed using commercially available CMOS process. The whole sensing procedure was conducted in the Taiwan Semiconductor Research Institute (TSRI). The chemicals, reagents, solvents used in this study were reagent-grade quality or higher level. The experimental procedure is divide into five parts: (1) Chemicals and materials; (2) Fabrication of the side-gated NBFET device; (3) Surface functionalization and biografting; (4) Fabrication of microfluidic channel; (5) Devices measuring and analyzing. These five parts are discussed in more details in the following section.

2.1. Chemicals and materials

Analytical-grade ethanol (C_2H_5OH, ≥99.8% in purity), 3-amino-propyl-triethoxy-silane [APTES; $H_2N(CH_2)_3Si(OC_2H_5)_3$, 221.37 g/mol], glutaraldehyde [GA; $OHC(CH_2)_3CHO$; 100.12 g/mol],

Preprints (www.preprints.org) | NOT PEER-REVIEWED | Posted: 7 December 2023 doi:10.20944/preprints202312.0419.v1

phosphate-buffered saline (PBS, 120 mM NaCl, 2.7 mM KCl, and 10 mM phosphate buffer; pH 7.4) were purchased from Sigma-Aldrich (St. Louis, MO, USA). A synthetic fluorescein isothiocyanate (FITC)-labeled DNA strand having the sequence of 5'-NH_2-ACGTCCCGCGCAGGA-3'-FITC was purchased from Blossom Biotechnologies, Taipei, Taiwan. To prevent chemical deterioration, APTES was stored in 4 °C environment , DNA and GA were stored in -20 °C environment after dilution.

2.2. Fabrication of the silicon NBFET

A schematic diagram of the fabricating flowchart of the NBFET device is depicted in Figure 1. To form the silicon NBFET sensors, commercially available 6-in. (100) silicon-on-insulator (SOI) wafers were used as the substrate [Figure 1(a)]. Firstly, a stack film of 30-nm-thick TEOS-oxide (SiO_2) and 100-nm-thick silicon nitride (Si_3N_4) were deposited sequentially on the substrate [Figure 1(b)], followed by the 1st lithography and etch process to define the stack film as an active region of the device [Figure 1(c)]. The lithography system used in this experiment was TRACK (TEL CLEAN-TRACK MK8) and I-line exposure system (Canon FPA-3000i5 stepper). The wafers were thermally grown for oxidation, making the exposed silicon substrate transformed to a 500-nm-thick SiO_2 film [Figure 1(d)]. On the other hand, the substrate which was covered by the SiO_2/ Si_3N_4 stack film remained the silicon film because of the nature of the high-density Si_3N_4 film that prevented the underlying silicon from oxidation. This local-oxidation of silicon process was often used as the isolation of MOS manufacturing. In addition, the linewidth of nanobelts were shrunk due to oxidant diffused laterally during this process. This phenomenon could induce the linewidth of nanobelts smaller than the critical width of the exposure system's capability.

The SiO_2/ Si_3N_4 stack film was removed after the oxidation process, and therefore a nanobelt was formed [Figure 1(e)]. The 2nd lithography process was then conducted, followed by As+ ion implantation and rapid thermal anneal to form the source, drain, and gate region. A stack layer of 100-nm-thick TEOS-oxide and 20-nm-thick Si_3N_4 was deposited sequentially to protect the device, and then the 3rd lithography and etch process were used to from contact hole. A 200-nm-thickAlSiCu alloy film was deposited by sputtering system, followed by the 4th lithography and metal etch process to define the electrode pad [Figure 1(f)]. Finally, the 5th lithography and Si_3N_4/TEOS-oxide film etch-back process was conducted to expose the nanobelts for biosensing purpose [Figure 1(g)]. To avoid the nanobelts degenerating, the completed biosensor devices was coated a photo-resist and stored in the clean room before using.

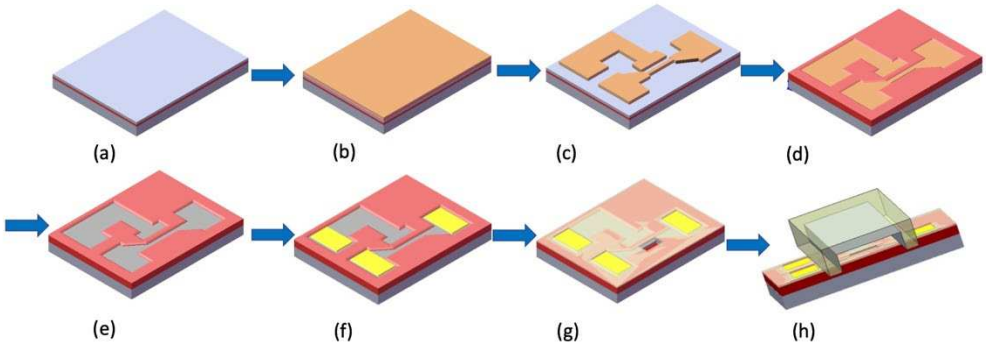

Figure 1. Schematic diagram of the fabricating flowchart of the NBFET device.

2.3. Surface functionalization and biografting

The fabrication of the NBFET sensors involved a series of surface functionalization to enable the attachment of biomolecules onto the nanobelt surfaces for biological sensing purposes. Prior to any surface chemical modification, the photoresist layer on the chips was removed by immersing them in a photoresist remover (EKC 830) at 90 °C for 15 minutes. Following this step, the chips underwent thorough cleansing and were subsequently dried. To introduce OH^- terminals on the nanowire surfaces, oxygen plasma treatment was administered for 5 minutes. Subsequently, the samples were

Preprints (www.preprints.org) | NOT PEER-REVIEWED | Posted: 7 December 2023 doi:10.20944/preprints202312.0419.v1

immersed in a 10% aqueous solution of APTES for 30 minutes at 37 °C, with the pH adjusted to 3.5 using 1 M HCl. After this, the samples were rinsed with deionized (DI) water and dried on a hot plate at 120 °C for 30 minutes. The surface reactions primarily involved the silanol groups present on the silicon nanobelt surface due to silicon dioxide formation. Notably, silanol groups exhibit excellent proton donor (H^+) and acceptor (SiO^-) properties, making them suitable for binding with APTES to form a self-assembled monolayer on the nanobelt surface, thereby completing the NH_2 surface functionalization [24]. Following the removal of excess alcohol, the amino groups were functionalized. To introduce aldehyde groups to the surface, GA was linked to the amino groups. The sample was immersed in a linker solution containing 2.5% GA for 30 minutes at room temperature and then rinsed with PBS solution. Figure 2 presents scheme of surface functionalization and biografting processes.

To bind the synthetic 15-mer single-stranded DNA to the nanobelt, a sequence dilution was conducted to provide a 10 nM solution of DNA using PBS buffer. One drop of a the DNA solution was then placed in the nanobelt, waiting for 1 hour to ensure completely binding, followed by a wash process to remove the unreacted DNA strands.

2.4. Fabrication of microfluidic channel

Before subjecting the NBFET biosensor to long-time record its electrical response in a liquid environment, it was necessary to prepare the experimental setup. To facilitate this, a microfluidic channel was fabricated, featuring a width of 50 μm. This channel was constructed using Polydimethylsiloxane (PDMS) and securely sealed on the sensor device through a special fixture tool. The microfluidic channel served as a conduit for the flow of fluids through the nanobelt, allowing precise volume control and manipulation of the sensing environment. This controlled flow of target liquids was a critical aspect of the experiment setup and was achieved using an automated syringe pump, specifically the Model 780270 from Kd Scientific, USA. This level of precision is crucial in long-time monitoring, particularly when studying the behavior of biosensor's stability and degradation in a liquid environment.

2.5. Devices measuring and analyzing

The fabricated nanobelt and NBFET surface morphology were observed by using tunneling electron microscope (TEM) and field-emission scanning electron microscope (FESEM), respectively. The electrical properties of the NBFET biosensor devices were characterized using an Agilent-4156C semiconductor parameter analyzer (Agilent Technologies, CA, USA). The drain current versus gate voltage (I_D–V_G) curves of the NBFET devices were recorded in each step to exam their performance. Secondary ion mass spectroscopy (SIMS) was used to analyze ions penetration into the silicon. Surface roughness was inspected using atomic force microscope (AFM).

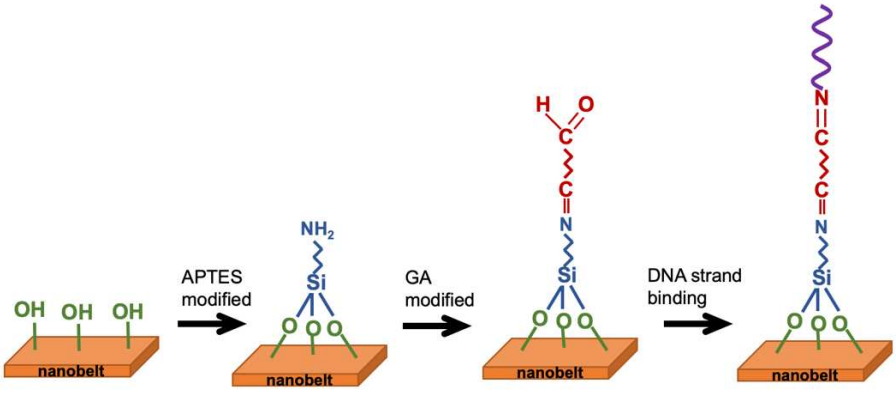

Figure 2. Schematic representation of surface functionalization and biografting steps.

Preprints (www.preprints.org) | NOT PEER-REVIEWED | Posted: 7 December 2023 doi:10.20944/preprints202312.0419.v1

3. Results and Discussions

We used a TEM (JEM-2010F, JOEL Ltd., Tokyo, Japan) to observe the structure of the nanobelt. Figure 3(a) presents a cross-sectional image of the silicon nanobelt, revealing key structural details. Notably, the width of the nanobelt underwent a significant reduction, diminishing from its original dimensions of 350 nm to a slender 150 nm. Moreover, the initial thickness of 50 nm experienced a substantial decrease to approximately 5 nm following the LOCOS processing, as visually demonstrated in the figure. It's imperative to underscore that the local-oxidation of silicon process, as shown in Figure 1(d), is of critical importance to the formation of the nanobelt. This transformation in the nanobelt's dimensions is intricately linked to the oxide thickness in the local-oxidation process. Not only does the oxidation process validate the complete oxidation of the underlying silicon, but also ensures the preservation of the nanobelt's original thickness. This meticulous control over the structural changes in the nanobelt plays a pivotal role in enhancing the sensitivity of the NBFET biosensor. The improved sensitivity of the NBFET sensor is attributed to the substantial reduction in dimensions while retaining a substantial detection region on the surface. This combination of factors contributes to the sensor's heightened capability to detect and respond to subtle changes in its surroundings.

The morphology of the NBFET device was demonstrated through FESEM (JSM-6700F, JOEL Ltd., Tokyo, Japan). Figure 3(b) presents top-view image of the NBFET device, including source, drain, side-gate, and nanobelt. The length of the nanobelt in our design was 30 μm-long. The side-gate was designed in the NBFET biosensor to provide an in- dividual gate voltage for each device, and hence ensure its controllable and stable properties.

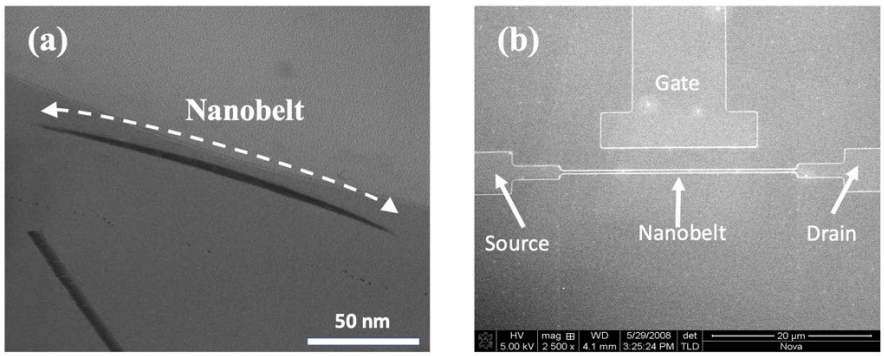

Figure 3. (a) Cross-sectional TEM images of the formed silicon nanobelt. (b) Top-view FESEM image of the NBFET structure.

To exam the electrical characteristics of the side-gates NBFET devices, the drain current versus gate voltage (I_D–V_G), as well as drain current versus drain voltage (I_D–V_D), were measured before biosensing applications. The I_D–V_G and I_D–V_D curves serve as crucial indices for assessing the characteristics of a transistor device. Prior to electrical measurements, PBS was introduced through the microfluidic channel and subsequently remained on the nanobelt surface. It is noteworthy that the detection area was selectively opened on a segment of the nanobelt, as depicted in Figure 1(g). The remaining portion of the entire device was shielded by a Si_3N_4/oxide film. In this configuration, only the nanobelt came into contact with PBS, ensuring that the gate, drain, and source electrodes remained unaffected by the solution. The fundamental electrical performance of the transistor device is of paramount importance, as it directly impacts the biosensor's sensitivity, limit of detection (LOD), as well as its stability and reliability when employed as a biosensor. In Figure 4(a), we present the I_D–V_G plot at V_D of 0.5 and 1 V, respectively. This plot illustrates the ability to switch the current I_D flowing through the nanobelt, from 10^{-11} to 10^{-6} A, at various side gate potentials. Under a substantial negative gate voltage, such as –2 V, the channel conduction is notably low. When applying a positive voltage to the gate, such as 2 V, it creates an electron channel, rendering the transistor a normally-on, and thus the current increases. In practice, the side gate can apply an electric field to the nanobelt,

Preprints (www.preprints.org) | NOT PEER-REVIEWED | Posted: 7 December 2023 doi:10.20944/preprints202312.0419.v1

thus influencing the energy band for the charge carriers. The sensor's practicality is further highlighted by the on/off current ratio, which approaches five orders of magnitude when V_D is applied on 1 V. The determined threshold voltage (V_t) can be extracted to approximately 0.5 V, and the subthreshold swing (SS) is calculated to be 150 mV/decade. This substantial ratio suggests the enhanced utility of the fabricated NBFET biosensors, which can be attributed to the heightened sensitivity.

Figure 4(b) depicts the I_D–V_D curves of the NBFET device across a range of applied V_G values, spanning from -1 to 6 V. It is observed that the I_D increases obviously when V_G is increasing, whereas only a modest increase with increasing V_D. The result of this figure highlights the distinctive behavior of I_D concerning V_D and V_G for the NBFET device, which indicates the primary factor influencing the current is the variation in V_G. Therefore, the judicious selection of an appropriate gate voltage becomes imperative to operate the device under the most favorable conditions for subsequent biosensing applications. Understanding the interplay between V_G, V_D, and I_D in this NBFET device is pivotal for optimizing its performance as a biosensor. By strategically adjusting the gate voltage, it becomes feasible to precisely modulate the device's current response, enhancing its sensitivity and reliability in biosensing applications.

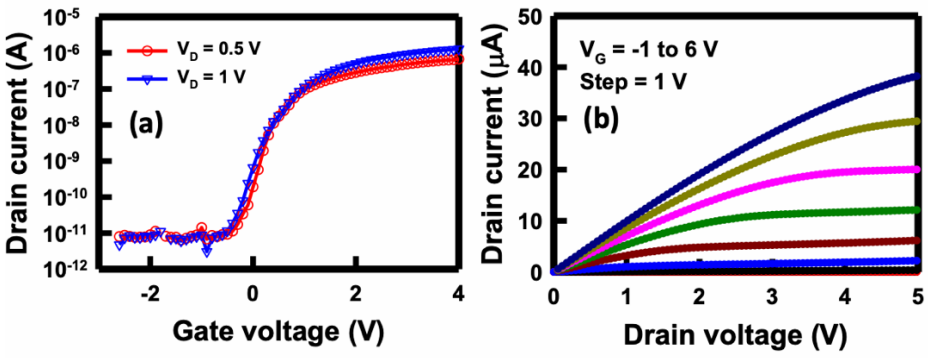

Figure 4. Fundamental electrical characteristics of the NBFET device. (a) I_D–V_G curves at V_D= 0.5 and 1 V, and (b) I_D–V_D curves at V_G from -1 to 6 V.

The stability of the NBFET device, especially when utilized as a biosensor in complex liquid environments, is a critical consideration. The challenges posed by extended exposure to buffer solutions, along with the presence of ions, necessitate a thorough investigation into the stability of the biosensor device. This endeavor is fundamental to ensuring the device's reliability and effectiveness in real-world biomedical applications, where precise and consistent results are of utmost importance.

Given these intricate challenges, it is imperative to conduct a time-dependent stability assessment of the NBFET device when immersed in a buffer solution. This evaluation allows us to gain insights into how the device's performance evolves over time in real conditions. Illustrated in Figure 5 are the I_D–V_D curves of the NBFET biosensor immersed in PBS over varying durations. Evidently, the curves gradually shift right with increasing immersion days. Notably, the SS experiences a slight change after 5 days, becoming significantly smaller after 10 days of immersion. This observation underscores the impact of the buffer solution on the electrical characteristics of the NBFET device, revealing a heightened degradation as the immersion duration extends. These findings emphasize the necessity of understanding and addressing the time-dependent stability challenges in biosensor applications.

Preprints (www.preprints.org) | NOT PEER-REVIEWED | Posted: 7 December 2023 doi:10.20944/preprints202312.0419.v1

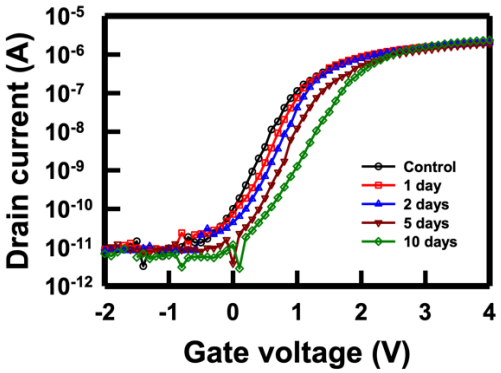

Figure 5. I_D–V_D curves of the NBFET biosensor immersed in PBS over varying durations.

To comprehend the underlying mechanism behind the degradation induced by the buffer solution, we conducted a thorough analysis of the electrical characteristics of NBFET biosensors immersed in PBS solutions with varying concentrations. Figure 6 illustrates the voltage shifts of NBFET devices immersed in original 10 mM (denoted as 1×) and diluted 1 mM (denoted as 0.1×) concentrations, respectively. The calculation of voltage shift involved utilizing the drain current associated with the control V_t value ($V_{t,\text{Control}}$) of the NBFET biosensor device as the baseline current. This reference current was then incorporated into the curves for different immersion durations to derive the immersed V_t value ($V_{t,\text{Immerse}}$). The formula for this calculation is as follows:

$$\text{Voltage shift} = (V_{t,Immerse} - V_{t,Control}) \quad \ldots\ldots\ldots\ldots\ldots\ldots\ldots\ldots (1)$$

The results show that, regardless of whether the devices were immersed in 1× or 0.1× solutions, the voltage shifts increased with prolonged immersion days, aligning with the trends observed in Figure 5. Remarkably, a higher magnitude of voltage shifts was observed in the 1× PBS sample compared to the 0.1×. This discrepancy can be attributed to the tenfold higher ion concentration in the 1× PBS compared to the 0.1×. From this, we infer that the primary cause of NBFET degradation is the penetration of ions into the nanobelt structure. This understanding sheds light on the critical role of ion penetration in the observed degradation of NBFET devices immersed in buffer solutions, further emphasizing the importance of addressing this challenge for enhanced device reliability and longevity.

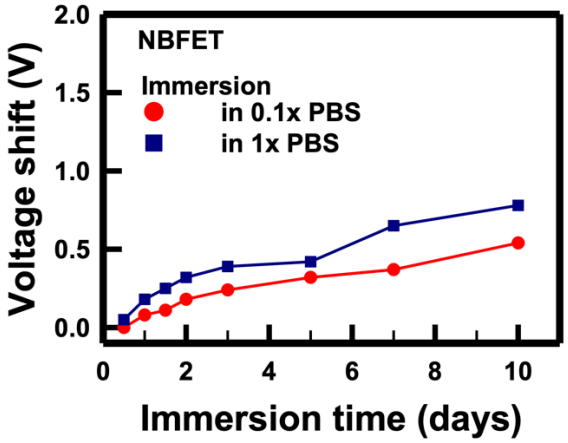

Figure 6. Voltage shifts of the NBFET biosensors immersed in PBS solutions with different concentrations over varying durations.

Preprints (www.preprints.org) | NOT PEER-REVIEWED | Posted: 7 December 2023 doi:10.20944/preprints202312.0419.v1

To elucidate the phenomenon of ion penetration during the immersion period, we employed SIMS (CAMECA IMS 7F, AMETEK, Inc., Gennevilliers, France) analysis for monitoring purposes. Analyzing the key ions present in the PBS buffer solution, namely sodium (Na^+), potassium (K^+), chlorine (Cl^-), and phosphorous (P^{3+}), we conducted a thorough investigation. Figure 7 depicts the SIMS depth profiles of these ions for samples immersed in PBS for durations ranging from 0.5 to 10 days. The results obtained highlight the penetration of Na^+ and K^+ ions into the substrate post-immersion, with no observable penetration for Cl^- and P^{3+} ions. Specifically, Na^+ ions exhibited slight penetration into the substrate after 2 days, intensifying from days 3 to 10. In contrast, noticeable penetration of K^+ ions was observed after 5 days of immersion. These findings from the SIMS analysis align with the previously discussed electrical properties of the NBFET devices.

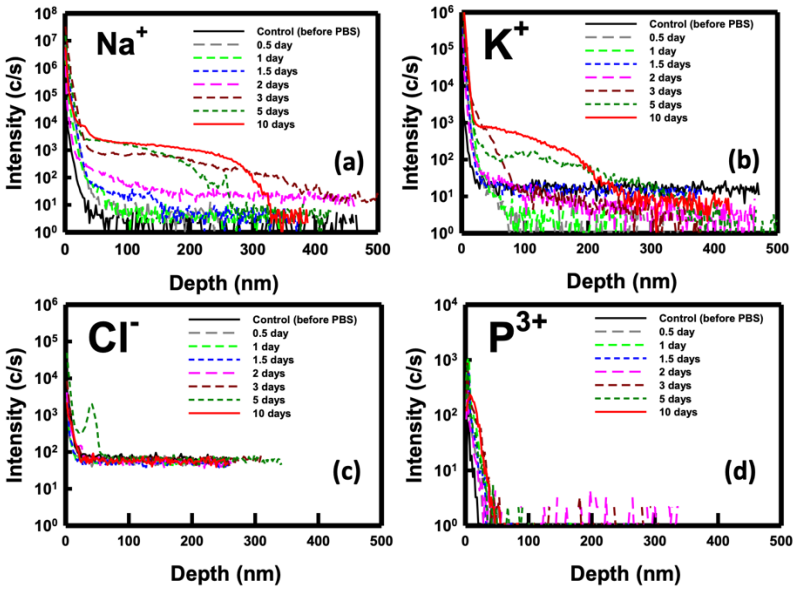

Figure 7. SIMS depth profile of the ions for the sample immersed in the PBS solution over various durations. (a) Sodium ions, (b) potassium ions. (a) chlorine ions, and (a) phosphorus ions.

The electrical performance of NBFET biosensors featuring APTES coating on the nanobelt surface was also assessed to evaluate their effectiveness following PBS immersion. In Figure 8, the voltage shifts of APTES-functionalized NBFET biosensors immersed in 1× and 0.1× PBS buffers are illustrated. Notably, for samples subjected to less than 5 days of immersion, APTES-functionalized NBFET devices exhibited smaller voltage shifts compared to their uncoated counterparts. However, the voltage shifts of APTES-functionalized NBFET devices showed a significant increase during immersion from 7 to 10 days. Furthermore, the discrepancy in voltage shifts between 1× and 0.1× PBS conditions was found to be smaller for the APTES-functionalized samples compared to the uncoated ones. This observation leads us to conclude that, within the initial 5 days of immersion, ions' penetration may influence the performance of NBFET devices. Beyond this period, however, ions' penetration is not the predominant mechanism causing voltage shifts in the APTES-coated samples. These findings underscore the temporal dynamics of APTES coating effectiveness in mitigating ion-induced effects on NBFET device performance.

Preprints (www.preprints.org) | NOT PEER-REVIEWED | Posted: 7 December 2023 doi:10.20944/preprints202312.0419.v1

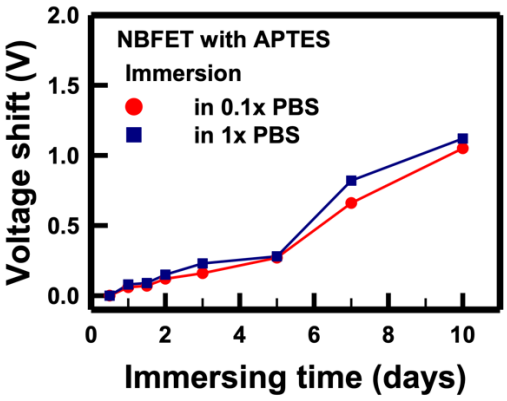

Figure 8. Voltage shifts of the APTES-functionalized NBFET biosensors immersed in PBS solutions with different concentrations over varying durations.

In Figure 9, AFM images depicting the APTES-coated samples are presented for intervals of 0, 3 days, and 5 days of PBS immersion. The presence of white spots in the images signifies chemical molecules binding to the surface. Following a 3-day immersion, the number of white spots noticeably increases. Notably, after 5 days of immersion, the size of these white spots undergoes a substantial increase, forming clusters on the sample surface. We hypothesize that these white clusters result from APTES peeling off after prolonged immersion in the PBS solution. This supposition aligns with the electrical measurement results showcased in Figure 8. Given the positively charged nature of the APTES film, the peeling off of the film induces a rightward shift in the I_D–V_G curve of the NBFET device, leading to an increase in V_t. This correlation between AFM observations and electrical measurements provides valuable insights into the impact of prolonged PBS immersion on the APTES-coated samples, further underlining the intricate dynamics between surface modifications and device performance.

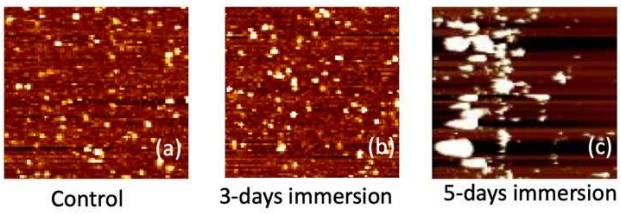

Figure 9. Surface AFM images of the APTES-coated samples for (a) control (0 day), (b) 3 days, and (c) 5 days of PBS immersion.

In Figure 10, fluorescence images depicting FITC-labeled DNA strands bonded to the SiO_2 line patterns are presented for immersion durations of 0, 3 days, and 5 days in PBS. The attachment of DNA strands to the SiO_2 line patterns was facilitated through amine and carboxyl interactions, achieved via the APTES and GA functionalization process. Notably, the control sample exhibits the highest and most distinct fluorescence intensity, indicating a high binding efficiency of DNA strands to the SiO_2 substrate. However, the fluorescence intensity decreases as the immersion duration increases. By integrating the results from AFM and fluorescence images, we can deduce that prolonged PBS immersion induces the peeling off of the APTES film, consequently degrading the binding efficiency of biomolecules. This comprehensive analysis underscores the intricate interplay between surface modifications, biomolecule binding, and the environmental factors affecting biosensor performance over time.

Preprints (www.preprints.org) | NOT PEER-REVIEWED | Posted: 7 December 2023 doi:10.20944/preprints202312.0419.v1

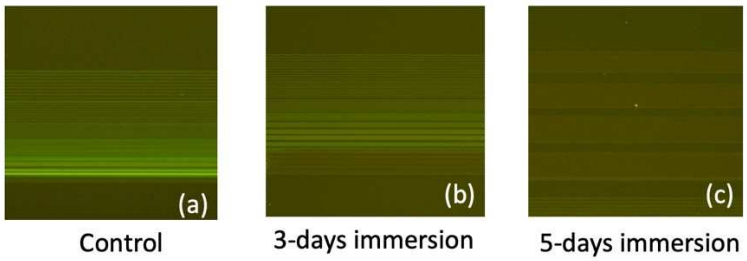

Figure 10. Fluorescence images of the FITC-labeled DNA strands bonded to the SiO_2 line patterns for PBS immersion durations of (a) control (0 day), (b) 3 days, and (c) 5 days.

4. Conclusions

This paper presents an exploration of the electrical properties of NBFET biosensor devices exposed to buffer solutions for extended durations. Fabricated through a CMOS-compatible manufacturing process, the NBFET biosensor features a nanobelt formed using the local oxidation of silicon technique. The dimensions of the nanobelt are 200 nm-wide, 30 μm-long, with a thickness down to 10 nm. Employing this technique, the NBFET device exhibits a remarkable five orders of magnitude in on/off current ratio and a subthreshold swing of 150 mV/decade.

Upon immersion in a buffer solution, the results indicate that the buffer solution accelerates the degradation of the transistor device, leading to an increase in threshold voltage shift with prolonged immersion. SIMS analysis further confirms the penetration of Na^+ and K^+ ions into the substrate after 5 days of PBS immersion. Additionally, for APTES-coated NBFET biosensor devices, PBS immersion is shown to cause the deterioration of surface functionalization.

In summary, the infiltration of the buffer solution into the device raises concerns regarding the reliability of the biosensor and potential deterioration of surface functionalization after prolonged immersion. This study sheds light on the dynamic behavior of NBFET devices in real-world conditions, emphasizing the importance of addressing these challenges for enhanced biosensor performance and longevity.

Funding: This research was funded by the Taiwan Ministry of Science and Technology, grant number MOST111-2221-E-167-022.

Institutional Review Board Statement: Not applicable.

Informed Consent Statement: Not applicable.

Acknowledgments: The authors would like to thank the Taiwan Semiconductor Research Institute for their technical support.

Conflicts of Interest: The funders had no role in the design of the study, the collection, analyses, or interpretation of data, the writing of the manuscript, or the decision to publish the results.

References

1. Huang, C. W.; Lin, C.; Nguyen, M. K.; Hussain, A.; Bui, X. T.; Ngo, H. H. A Review of Biosensor for Environmental Monitoring: Principle, Application, and Corresponding Achievement of Sustainable Development Goals. *Bioengineered.* **2023**, 14, 58. https://doi.org/10.1080/21655979.2022.2095089
2. Zhang, S. P.; Huang, Y. T.; Ren, H. Z.; Chen, Y. J.; Yan, S. S.; Dai, H.; Lv, L. Facile and Portable Multimodal Sensing Platform Driven by Photothermal-Controlled Release System for Biomarker Detection. *Biosens Bioelectron.* **2023**, 235. https://doi.org/10.1016/j.bios.2023.115413
3. Quazi, S. Application of Biosensors in Cancers, an Overview. *Front Bioeng Biotech.* **2023**, 11. https://doi.org/10.3389/fbioe.2023.1193493
4. Wu, C. C. Polycrystalline Silicon Nanowire Field Effect Transistor Biosensors for Sars-Cov-2 Detection. *J Electrochem Soc.* **2022**, 169. https://doi.org/10.1149/1945-7111/ac80d6

Preprints (www.preprints.org) | NOT PEER-REVIEWED | Posted: 7 December 2023 doi:10.20944/preprints202312.0419.v1

5. Shetti, N. P.; Bukkitgar, S. D.; Reddy, K. R.; Reddy, C. V.; Aminabhavi, T. M. Zno-Based Nanostructured Electrodes for Electrochemical Sensors and Biosensors in Biomedical Applications. *Biosens Bioelectron.* **2019**, 141. https://doi.org/10.1016/j.bios.2019.111417
6. Ding, M. L.; Zhang, S. L.; Wang, J. E.; Ding, Y.; Ding, C. F. Ultrasensitive Ratiometric Electrochemiluminescence Sensor with an Efficient Antifouling and Antibacterial Interface of Psbma@Sio-Mxene for Oxytetracycline Trace Detection in the Marine Environment. *Analytical chemistry.* **2023**, 95, 16327. https://doi.org/10.1021/acs.analchem.3c03555
7. Sukjee, W.; Sangma, C.; Lieberzeit, P. A.; Ketsuwan, K.; Thepparit, C.; Chailapakul, O.; Ngamrojanavanich, N. Ev71 Virus Induced Silver Nanoparticles Self-Assembly in Polymer Composites with an Application as Virus Biosensor. *Sensor Actuat B-Chem.* **2023**, 393. https://doi.org/10.1016/j.snb.2023.134324
8. Parichenko, A.; Choi, W.; Shin, S.; Schlecht, M.; Gutierrez, R.; Akbar, T. F.; Werner, C.; Lee, J. S.; Ibarlucea, B.; Cuniberti, G. Hydrogel-Gated Silicon Nanotransistors for Sars-Cov-2 Antigen Detection in Physiological Ionic Strength. *Adv Mater Interfaces.* **2023**, https://doi.org/10.1002/admi.202300391
9. Hayashi, H.; Fujita, M.; Kuroiwa, S.; Ohashi, K.; Okada, M.; Shibasaki, F.; Osaka, T.; Momma, T. Semiconductor-Based Biosensor Exploiting Competitive Adsorption with Charged Pseudo-Target Molecules for Monitoring 5-Fluorouracil Concentration in Human Serum. *Sensor Actuat B-Chem.* **2023**, 395. https://doi.org/10.1016/j.snb.2023.134495
10. Ren, Q. Q.; Jiang, L. Y.; Ma, S. H.; Li, T.; Zhu, Y.; Qiu, R.; Xing, Y.; Yin, F.; Li, Z. G.; Ye, X. Y.; Zhang, Y. P.; Zhang, M. Multi-Body Biomarker Entrapment System: An All-Encompassing Tool for Ultrasensitive Disease Diagnosis and Epidemic Screening. *Adv Mater.* **2023,** 35. https://doi.org/10.1002/adma.202304119
11. Shariati, M.; Sadeghi, M.; Khoshkhoo, S. M.; Azimi, N. Materialization of a Novel Decorated Nanowire Biosensor Platform Based on Field Effect Transistor under Electrochemical Gate Modulation. *J Electrochem Soc.* **2023**, 170. https://doi.org/10.1149/1945-7111/ace336
12. Xing, J.; Dong, Q. Y.; Ding, Q.; Yang, X.; Yuan, R.; Yuan, Y. L. Photoactive Conjugated Microporous Polymer/Carbon Nanotube Coupled with T-Junction Recycling Dual-Strand Displacement Amplification for Sensing N-Gene of Covid-19. *Sensor Actuat B-Chem.* 2023, **376**. https://doi.org/10.1016/j.snb.2022.132974
13. Monavari, S. M.; Marsusi, F.; Memarian, N.; Qasemnazhand, M. Carbon Nanotubes and Nanobelts as Potential Materials for Biosensor. *Scientific reports.* **2023**, 13. https://doi.org/10.1038/s41598-023-29862-9
14. Bhattacharyya, I. M.; Cohen, S.; Shalabny, A.; Bashouti, M.; Akabayov, B.; Shalev, G. Specific and Label-Free Immunosensing of Protein-Protein Interactions with Silicon-Based Immunofets. *Biosens Bioelectron.* **2019**, 132, 143. https://doi.org/10.1016/j.bios.2019.03.003
15. Manimekala, T.; Sivasubramanian, R.; Dharmalingam, G. Nanomaterial-Based Biosensors Using Field-Effect Transistors: A Review. *J Electron Mater.* **2022**, 51, 1950. https://doi.org/10.1007/s11664-022-09492-z
16. Zhang, H.; Kikuchi, N.; Ohshima, N.; Kajisa, T.; Sakata, T.; Izumi, T.; Sone, H. Design and Fabrication of Silicon Nanowire-Based Biosensors with Integration of Critical Factors: Toward Ultrasensitive Specific Detection of Biomolecules. *ACS appl mater interfaces.* **2020**, 12, 51808. https://doi.org/10.1021/acsami.0c13984
17. Kazemi, N.; Abdolrazzaghi, M.; Light, P. E.; Musilek, P. In-Human Testing of a Non-Invasive Continuous Low-Energy Microwave Glucose Sensor with Advanced Machine Learning Capabilities. *Biosens Bioelectron.* **2023**, 241. https://doi.org/10.1016/j.bios.2023.115668
18. Das, S.; Saxena, K.; Tinguely, J. C.; Pal, A.; Wickramasinghe, N. L.; Khezri, A.; Dubey, V.; Ahmad, A.; Perumal, V.; Ahmad, R.; Wadduwage, D. N.; Ahluwalia, B. S.; Mehta, D. S. Sers Nanowire Chip and Machine Learning-Enabled Classification of Wild-Type and Antibiotic-Resistant Bacteria at Species and Strain Levels. *ACS appl mater interfaces.* **2023**, 15, 24047. https://doi.org/10.1021/acsami.3c00612
19. Ouhibi, A.; Raouafi, A.; Lorrain, N.; Guendouz, M.; Raouafi, N.; Moadhen, A. Functionalized Sers Substrate Based on Silicon Nanowires for Rapid Detection of Prostate Specific Antigen. *Sensor Actuat B-Chem.* **2021**, 330. https://doi.org/10.1016/j.snb.2020.129352
20. Pradhan, S.; Albin, S.; Heise, R. L.; Yadavalli, V. K. Portable, Disposable, Biomimetic Electrochemical Sensors for Analyte Detection in a Single Drop of Whole Blood. *Chemosensors.* **2022**, 10. https://doi.org/10.3390/chemosensors10070263
21. Das, N.; Roychaudhuri, C. Reliability Study of Nanoporous Silicon Oxide Impedance Biosensor for Virus Detection: Influence of Surface Roughness. *IEEE T Device Mat Re.* **2015**, 15, 402. https://doi.org/10.1109/Tdmr.2015.2457452
22. Elgiddawy, N.; Ren, S. W.; Yassar, A.; Louis-Joseph, A.; Sauriat-Dorizon, H.; El Rouby, W. M. A.; El-Gendy, A. O.; Farghali, A. A.; Korri-Youssoufi, H. Dispersible Conjugated Polymer Nanoparticles as Biointerface Materials for Label-Free Bacteria Detection. *ACS appl mater interfaces.* **2020**, 12, 39979. https://doi.org/10.1021/acsami.0c08305

Preprints (www.preprints.org) | NOT PEER-REVIEWED | Posted: 7 December 2023 doi:10.20944/preprints202312.0419.v1

23. Tian, M.; Wang, J. H.; Li, C. H.; Wang, Z. X.; Liu, G. F.; Lv, E. G.; Zhao, X. F.; Li, Z.; Cao, D. Y.; Liu, H. L.; Zhang, C.; Xu, S. C.; Man, B. Y. Qualitative and Quantitative Detection of Microcystin-Lr Based on Sers-Fet Dual-Mode Biosensor. *Biosens Bioelectron.* **2022**, 212. https://doi.org/10.1016/j.bios.2022.114434
24. Kenaan, A.; Li, K. Z.; Barth, I.; Johnson, S.; Song, J.; Krauss, T. F. Guided Mode Resonance Sensor for the Parallel Detection of Multiple Protein Biomarkers in Human Urine with High Sensitivity. *Biosens Bioelectron.* **2020**, 153. https://doi.org/10.1016/j.bios.2020.112047

Disclaimer/Publisher's Note: The statements, opinions and data contained in all publications are solely those of the individual author(s) and contributor(s) and not of MDPI and/or the editor(s). MDPI and/or the editor(s) disclaim responsibility for any injury to people or property resulting from any ideas, methods, instructions or products referred to in the content.